THE JOURNAL OF BIOLOGICAL CHEMISTRY
Vol. 278, No. 46, Issue of November 14, pp. 45730–45736, 2003

Printed in U.S.A.

Solution Structure of the Plant Disease Resistance-triggering Protein NIP1 from the Fungus *Rhynchosporium secalis* Shows a Novel β-Sheet Fold*

Received for publication, July 30, 2003, and in revised form, August 27, 2003
Published, JBC Papers in Press, August 27, 2003, DOI 10.1074/jbc.M308304200

Klaas A. E. van't Slot‡§, Harrold A. van den Burg¶, Cathelijne P. A. M. Kloks‖, Cornelis W. Hilbers‖, Wolfgang Knogge‡‡, and Christina H. M. Papavoine‖§§¶¶**

*From the ‡Laboratory of Phytopathology, Department of Plant Sciences, Wageningen University, Binnenhaven 5, NL-6709 PD Wageningen, The Netherlands, ¶Laboratory of Biochemistry, Department of Biomolecular Sciences, Wageningen University, Dreijenlaan 3, NL-6703 HA Wageningen, The Netherlands, the ‖Department of Biophysical Chemistry, NSR Center, University of Nijmegen, NL-6500 HC Nijmegen, The Netherlands, the **School of Agriculture and Wine, The University of Adelaide, Glen Osmond, SA 5064, Australia, and the §§Medicinal Chemistry, AstraZeneca R&D Mölndal, S-431 83 Mölndal, Sweden*

Activation of the disease resistance response in a host plant frequently requires the interaction of a plant resistance gene product with a corresponding, pathogen-derived signal encoded by an avirulence gene. The products of resistance genes from diverse plant species show remarkable structural similarity. However, due to the general paucity of information on pathogen avirulence genes the recognition process remains in most cases poorly understood. NIP1, a small protein secreted by the fungal barley pathogen *Rhynchosporium secalis*, is one of only a few fungal avirulence proteins identified and characterized to date. The defense-activating activity of NIP1 is mediated by barley resistance gene *Rrs1*. In addition, a role of the protein in fungal virulence is suggested by its nonspecific toxicity in leaf tissues of host and non-host cereals as well as its resistance gene-independent stimulatory effect on the plant plasma membrane H^+-ATPase. Four naturally occurring NIP1 isoforms are characterized by single amino acid alterations that affect the different activities in a similar way. As a step toward unraveling the signal perception/transduction mechanism, the solution structure of NIP1 was determined. The protein structure is characterized by a novel fold. It consists of two parts containing β-sheets of two and three anti-parallel strands, respectively. Five intramolecular disulfide bonds, comprising a novel disulfide bond pattern, stabilize these parts and their position with respect to each other. A comparative analysis of the protein structure with the properties of the NIP1 isoforms suggests two loop regions to be crucial for the resistance-triggering activity of NIP1.

Plant disease resistance frequently results from the specific interaction of disease resistance (*R*) genes with corresponding pathogen avirulence (*Avr*) genes. When an *R* gene product recognizes the matching microbial *Avr*-dependent signal, plant defense reactions are activated to arrest further pathogen development. In recent years, many *R* genes have been characterized from various plant species, their products forming five classes of proteins with common structural motifs such as leucine-rich repeat domains, nucleotide-binding sites, leucine-zipper domains or domains similar to the cytoplasmic Toll/interleukin-1 receptor (1). Furthermore, studies on the signal transduction components that play a role in plant disease resistance have uncovered remarkable similarities with innate immunity pathways in insects and mammals (2).

Originating from very diverse pathogens the products of *Avr* genes, with the exception of the *Xanthomonas AvrBs3* gene family, lack such structural similarities. However, the increasing number of AVR proteins for which an impact on virulence has been demonstrated (3) suggests a common genuine function. In the broader sense, these proteins are produced by pathogens to allow or optimize development on the host. Their secondary role as specific signals in plant resistance triggering thus appears to be a function of the recognition capability of the plant. This is best described by the "guard hypothesis," which assumes that AVR proteins target host proteins to modulate critical plant activities. These host targets are "guarded" by R proteins, which initiate defense reactions when their "guardees" are disturbed by AVR proteins (1, 4). Currently, the tomato Pto kinase (4) and the RIN4 protein of *Arabidopsis thaliana* (5) best exemplify this scenario. According to the model, Pto is part of a general host defense-signaling pathway. The R protein Prf recognizes the interaction of Pto with bacterial AvrPto, which suppresses this pathway. RIN4 is a negative regulator of basal defense responses, an activity that is enhanced upon interaction with bacterial AvrB or AvrRpm1. RIN4 integrity is guarded by the *A. thaliana* RPM1 protein, which hence "recognizes" two different AVR proteins targeting the same plant factor.

More than 40 *Avr* genes from bacterial, but only very few from fungal, plant pathogens have been characterized. Most bacterial AVR proteins that are transferred into host cells via the bacterial type III secretion system (6) and the product of the *Avr-Pita* from the rice pathogen *Magnaporthe grisea* (7) have intracellular targets. In contrast, the AVR proteins from the tomato pathogen *Cladosporium fulvum* and from the barley pathogen *Rhynchosporium secalis* function extracellularly as

* The costs of publication of this article were defrayed in part by the payment of page charges. This article must therefore be hereby marked "*advertisement*" in accordance with 18 U.S.C. Section 1734 solely to indicate this fact.

The atomic coordinates and structure factors (code 1KG1) have been deposited in the Protein Data Bank, Research Collaboratory for Structural Bioinformatics, Rutgers University, New Brunswick, NJ (http://www.rcsb.org/).

The proton and nitrogen resonance assignments have been deposited in the BioMagnetic Resonance Bank data base (accession code 5199).

§ Supported by a grant from the Deutsche Forschungsgemeinschaft.

‡‡ Supported by a grant from the Deutsche Forschungsgemeinschaft. To whom correspondence should be addressed. Tel.: 61-8-8303-6822; Fax: 61-8-8303-7109; E-mail: wolfgang.knogge@adelaide.edu.au.

¶¶ Supported by a grant from the Swedish Natural Science Research Council.

elicitors of plant defense reactions (8). High affinity binding sites for two of the AVR proteins, AVR9 from *C. fulvum* (9) and NIP1 from *R. secalis*,[1] have been identified, although on membranes of both resistant and susceptible host plants as well as of related non-host species. In addition, the tomato Cf-9 protein that recognizes AVR9 without direct physical interaction (10) was recently found to be part of a membrane-associated protein complex (11). Nevertheless, the mechanism of AVR protein perception and signal transduction into the host cell is still not fully understood.

The *NIP1* gene of *R. secalis* encodes an 82-amino acid protein, which upon cleavage of a signal peptide yields a 60-amino acid mature protein that contains 10 cysteine residues (12) in five intramolecular disulfide bonds (13). Application of NIP1 to leaves of barley lines carrying the *R* gene, *Rrs1*, but not of lines lacking this gene, results in the induction of defense reactions (14). In addition, NIP1 has a virulence-associated function; independent of the plant genotype it stimulates the formation of necrotic lesions, a process that appears to be based on an indirect stimulation of the plant plasma membrane H^+-ATPase activity (15, 16).

All fungal races avirulent on *Rrs1*-barley carry and express the *NIP1* gene. In contrast, virulent races either lack the gene or carry alleles containing point mutations that translate into single amino acid alterations (12). To date four isoforms of NIP1 (denominated types I–IV) have been characterized that differ significantly in their biological activities (17). Understanding the effect of the amino acid differences between the four types of NIP1 on their function is an important step toward the elucidation of resistance triggering. To obtain more insight into the structure-function relationships, the three-dimensional structure of NIP1, type I, was solved using NMR spectroscopy. The resulting structure shows a novel protein fold that consists of two parts comprising β-sheets. By integrating the structural information with the results from binding and biological activity studies using the four NIP1 isoforms, a model is presented for NIP1 perception in the interaction between *R. secalis* and its host plant, barley.

EXPERIMENTAL PROCEDURES

Sample Preparation—For ^{15}N labeling of the protein, *Escherichia coli* strain BL21 carrying the pQE30-NIP1 vector (13) was grown in 5 liters of minimal medium (18) consisting of M9 salts, 20% glucose, Fe^{2+} (5 ng liter^{-1}) and thiamine (500 ng liter^{-1}). $^{15}NH_4Cl$ (ARL, Groningen, The Netherlands) was used as the sole nitrogen source. When bacterial cultures reached an A_{600} of 0.5, IPTG was added to a final concentration of 2 mM, and cells were harvested after incubation for 6 h at 37 °C. Following the protein isolation protocol described previously (13), 7.2 mg of [^{15}N]NIP1 were obtained from inclusion bodies. The ^{15}N incorporation was shown to be 97% with MALDI-TOF MS.[2] The elicitor activity of the labeled protein did not differ from that of unlabeled NIP1 (data not shown).

Disulfide Bond Assignments—Native NIP1, type I (80 μg; molecular mass = 6433.3 Da), was dissolved in 10 μl of 0.1 M citrate buffer (pH 3) containing 6 M guanidine HCl (GuCl) to facilitate the accessibility of the five disulfide bridges (19). Partial reduction was performed with a 5 molar excess of tris(2-carboxyethyl)phosphine (TCEP), a reagent that has proven to be an excellent reducing agent for disulfides at acidic pH (19). This reaction mixture was incubated at various temperatures for 15 min, directly followed by the addition of 4–5 μl of 0.1 M 1-cyano-4-dimethylaminopyridinium tetrafluoroborate, which resulted in cyanylation of the free sulfhydryl groups. An alternative alkylation reagent, *N*-ethylmaleimide, was used to achieve a better HPLC separation of singly reduced peptides. The partially reduced NIP1 mixture was separated by reversed-phase HPLC on a Delta Pak C_{18} column (150 × 3.9 mm, 300 Å, 5 μm, Waters Corp., Milford, MA) using 0.1% (v/v) trifluoroacetic acid in acetonitrile as eluting solvent. After purification the masses of the corresponding peptides were determined by MALDI-TOF MS. The singly reduced peptides were freeze-dried and subjected to chemical cleavage by adding 16 μl of 1 M aqueous NH_4OH (pH 10) containing 1.5 M GuCl. After 1 h at ambient temperature the samples were air-dried in a Speed Vac system. The remaining cystines were completely reduced by adding 4 μl of TCEP at pH 3. The resulting peptide fragments were further analyzed by mass spectrometry to assign the disulfide bonds (19–21).

Molecular masses were determined by MALDI-TOF MS on a Perseptive Biosystems Voyager DE-RP. A saturated matrix solution (α-cyano-4-hydroxycinnnamic acid, Aldrich) was freshly prepared in acetonitrile/water/TFA (50/50/1, v/v/v). One μl of each peptide sample was mixed with 1 μl of matrix solution on the MALDI target plate. External calibration was performed with a tryptic digest of the C116S mutant of 4-hydroxybenzoate 3-monooxygenase (EC 1.14.13.2) using fragments with calculated $[M + H]^+$ of 1099.6 Da and 2086.2 Da, bovine insulin (5734.6 Da) and bovine cytochrome *c* (12230.9 Da).

NMR Experiments—The NMR experiments were performed on Bruker DMX 600 and Varian Inova 500 and 600 spectrometers equipped with a pulsed-field gradient unit and triple resonance probe. The concentration of the NIP1 sample was 2 mM. The spectra were acquired at 25 °C and pH 6.0 (pH meter reading). Three-dimensional ^{15}N-edited NOESY (80 and 150 ms mixing time), ^{15}N-edited TOCSY (30 ms mixing time), ^{15}N HMQC-NOESY-GHSQC (150 ms mixing time), two-dimensional ^1H-^{15}N HSQC, ^1H COSY (H_2O and D_2O), ^1H NOESY (H_2O and D_2O, 80 and 150 ms mixing time), and ^1H TOCSY (H_2O and D_2O, 25 ms mixing time) spectra were used for the assignments. The spectra were processed using the NMRPipe program (22) on Silicon Graphics workstations. The data were interpreted using the program XEASY (23). Resonances were assigned following the standard strategy (24). Spectra were calibrated relative to tetramethylsilane (25). $^3J_{NH\text{-}H\alpha}$ coupling constants were determined in three-dimensional HNHA (26), two-dimensional HMQC-J (27), and three two-dimensional MJ-HMQC (28) spectra, $^3J_{N\text{-}H\alpha}$ coupling constants from a three-dimensional HNHB experiment. Two-dimensional NOESY and TOCSY experiments were analyzed as well. In the HMQC-J and the MJ-HMQC spectra the coupling constants were determined from the in-phase doublets in the ^{15}N dimension using the fitting procedure INFIT (29).

Steady-state ^1H-^{15}N NOE values, R1 and R2 ^{15}N relaxation times, were determined using gradient enhanced sensitivity pulse sequences (30). Spectra were acquired on a 500 MHz Varian Inova spectrometer. Two pairs of NOE experiments were recorded with (NOE) and without (NONOE) the use of ^1H saturation applied before the start of the experiment, respectively. Series of R1, with time delays of 15, 45, 105, 200, 400, 600, 800, 1000, 1300, 2000 ms, and R2, with time delays of 8.2, 24.6, 41, 57.5, 73.9, 90.3, 121.3, 172.4, 238, 320 ms, experiments were collected. NOE spectra were acquired using 2048 × 170 complex points. The R1 and R2 spectra were obtained using 2048 × 300 complex points. The relaxation parameters were determined from the peak heights. Data were analyzed using the Modelfree software (31) and reduced spectral density mapping (30).

Slowly exchanging amide protons were determined from the NH resonances from the fingerprint region cross peaks present in a TOCSY, COSY, and NOESY, recorded at 298 K of a NIP1 sample that was fully protonated and lyophilized. The spectra were recorded after dissolving the sample in D_2O within the first 12 h of exchange. These slow exchanging amides are thought to arise from strong hydrogen bonds within the structure.

Structure Calculation—Quantitative distance constraints were obtained from the three-dimensional ^{15}N NOESY HSQC (80 ms mixing time), HMQC-NOESY-GHSQC (150 ms mixing time), and the two-dimensional NOESY (D_2O, 80 ms mixing time). Distances (upper limits) were calibrated using the program DYANA (32). Since DYANA only calibrates upper limits, lower limits were introduced at a later stage. Interstrand d_{NN} and sequential $d\alpha_N$ and $d\alpha\alpha$ distances (taken from the thus far calculated structures) were used for the calibration of the HMQC-NOESY-GHSQC, three-dimensional NOESY HSQC, and NOESY spectrum, respectively. Lower limits were set by shortening the distances *r* by 20%. Stereo-specific assignments and angle restraints for NIP1 were obtained from a quantitative analysis of the various *J*-coupling spectra. Structures were calculated using 34 ϕ and 11 φ angle

[1] K. A. E. van't Slot and W. Knogge, unpublished results.

[2] The abbreviations used are: MALDI-TOF MS, matrix-assisted laser desorption-ionization time-of-flight mass spectroscopy; COSY, correlation spectroscopy; HMQC, heteronuclear multiple quantum coherence; HSQC, heteronuclear single quantum coherence; GHSQC, gradient-selected HSQC; NIP1, necrosis-inducing protein 1; NOE, nuclear Overhauser effect; NOESY, nuclear Overhauser and exchange spectroscopy; TCEP, tris(2-carboxyethyl)phosphine; TOCSY, total correlation spectroscopy; GuCl, guanidine HCl; HPLC, high performance liquid chromatography.

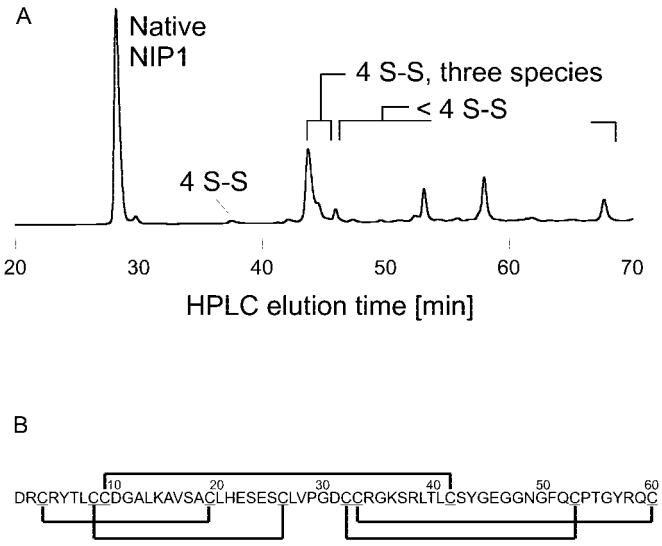

FIG. 1. **Assignment of disulfide bonds.** *A*, HPLC separation of NIP1 and its partially reduced/cyanylated isomers at 37 °C. The peaks annotated *4 S-S* represent singly reduced/cyanylated isomers as determined by MALDI-TOF. *B*, pattern of intramolecular disulfide bridges in NIP1.

constraints and 740 distance constraints.

The slowly exchanging amide protons resulted in 28 H-bonds. Constraints for the disulfide bridges were added according to the experiment described above. During the structure calculations, 24 lower limits of 4 Å were included, corresponding to NOEs not present in the spectra.

Resonance Assignments and Coordinates—The complete proton and nitrogen resonance assignments have been deposited in the BioMagnetic Resonance Bank data base (accession code 5199). Coordinates have been deposited in the Protein Data Bank (accession code 1KG1).

RESULTS

Assignment of Disulfide Bonds—NIP1 contains five intramolecular disulfide bridges (13). Determination of its disulfide bridge structure was performed according to the methods described earlier (19). Native NIP1 was partially reduced using the water-soluble reagent TCEP. The reactions were performed in 6 M GuCl to facilitate the accessibility of the five disulfide bridges. In contrast to results reported previously (19, 33), the disulfide bonds did not appear to be equally accessible to TCEP in 6 M GuCl. One disulfide bond opened significantly easier than the remaining four. After HPLC separation of the reaction mixture (Fig. 1*A*), four singly reduced peptides were identified by MALDI-TOF MS. Mass spectroscopy proved the other fragments to have more than one disulfide bond reduced. The fifth singly reduced NIP1 peptide could not be detected, also not by using the alkylation reagent *N*-ethylmaleimide as an alternative for the cyanylation reaction (33). Mass determination always resulted in the identification of two of the three expected mass peaks (Table I). β-Elimination, a common side reaction (34), was less frequently observed than reported by others (19). Interpretation of the results led to the disulfide pattern presented in Fig. 1*B*.

NMR Results and Structure Determination—The quality of the data obtained in the NMR experiment is exemplified in Fig. 2, which presents the $^{15}N,^{1}H$ HSQC spectrum of 2.0 mM NIP1 recorded at pH 6 and 298 K. The spectrum shows a very good dispersion for all backbone amide ^{15}N-H cross-peaks, indicative of a well structured protein. From NOESY spectra, the assigned H-bonds, the assigned disulfide bridge information and the torsion angle measurements, 785 restraints were derived, leading to 13.1 restraints per residue (Fig. 3). On the basis of these restraints, 100 structures were calculated using the program DYANA (32). The 25 structures with the lowest target function and no distance violations larger than 0.5 Å were selected. Fig. 4*A* shows a superposition of the backbone atoms (N, Cα, C′) of residues 3–11, 14–45, and 51–60. The structure of NIP1 reveals two "domains" or parts (Fig. 4*B*).

The energetic and geometric statistics of the best 25 structures are presented in Table II. All structures are in good agreement with the experimental restraints. No structures showed consistent (>60% of all structures) NOE structure violations larger than 0.2 Å or dihedral angle restraints larger than 3°. Ramachandran analysis of the ensemble showed that 97% of the residues lie in the allowed regions. From the relaxation measurements, R1 and R2 rates and NOE values were determined and subsequently used to calculate spectral densities, employing the reduced spectral density mapping method (30). Fig. 5 presents the spectral densities, which were calculated at zero, ω_N and ω_H (50.7 and 500 MHz, respectively). From a comparison of the χ^2 values of the "isotropic" and "anisotropic" Modelfree analyses followed that the dynamics of NIP1 can be described with an isotropic model. The overall rotational correlation time τ_c derived from the mean value of the R2/R1 ratio was determined to be 4.8 ns. The reduced spectral density mapping indicates that the dynamic properties are quite similar for most residues in the protein (Fig. 5). The behavior of residues with spectral density values strongly different from the average can be explained by increased internal flexibility or conformational exchange (see below).

DISCUSSION

The NIP1 Structure—NIP1 has a well defined structure predominantly formed by β-strands (Figs. 4, *A* and *B*). It consists of two parts that have a well defined mutual orientation. The five intramolecular disulfide bonds play a major role in the NIP1 fold, providing a high level of stability. This was illustrated by circular dichroism measurements, which showed that most of the secondary structure elements are preserved even at 100 °C.[3] The disulfide bond pattern determined with the "partial reduction procedure" was confirmed by the NMR measurements.

A closer look at the NIP1 structure reveals that if the N-terminal two residues and β5 were discarded, the structure can be considered as a tandem repeat of similar structural parts. Each part contains four cysteines in structurally equivalent positions (Cys^8, Cys^9, Cys^{19}, and Cys^{26} in the first, and Cys^{32}, Cys^{33}, Cys^{42}, and Cys^{53} in the second part). The first and fourth cysteines of each domain form a disulfide bond, whereas the second cysteine of the first (Cys^9) and the third cysteine of the second part (Cys^{42}) form a disulfide bond between the parts. The remaining two cysteines (Cys^{19} and Cys^{33}) form disulfides with the cysteines at the N and C termini (Cys^3 and Cys^{60}, respectively), and it can readily be imagined how longer structures can be formed as tandem repeats of these structural motifs.[4] However, no higher repeat number proteins were found in the data base.

With the exception of the first two amino acids at the N terminus, loop I and in particular loop III, the structure of NIP1 is rather rigid (Fig. 4, *A* and *B*). This is mainly a consequence of the presence of the five disulfide bonds. Starting at the N terminus, the first β-sheet is formed by residues 4–8 (β1) and 16–20 (β2). By forming a covalent linkage between the flexible N-terminal part of the protein and β2, thereby crossing the first β-sheet, the disulfide bond between Cys^3 and Cys^{19} stabilizes this β-sheet. However, the amide protons in this β-sheet exchange faster than those in other parts of the protein (data not shown) indicating that conformational exchange oc-

[3] V. Li and W. Knogge, unpublished results.
[4] A. Murzin, personal communication.

TABLE I

Expected and observed (in italics) m/z values for peptide fragments resulting from the indicated singly reduced/cleaved disulfide bridges

Fragments smaller than 1000 *m/z* were not detected due to the settings of the MALDI-TOF MS mass gate. itz, iminothiazolidine derivative of N-terminal cysteine in cleavage products.

Reduction of disulfide pair	N terminus to 1st Cys	itz-1st Cys to 2nd Cys	itz-2nd Cys to C terminus	β-Elimination N terminus	β-Elimination C terminus
Cys^{3}-Cys^{19}	289.3	1699.0	4537.1	1911.3	6158.0
		1698.1	*4541.4*	*1910.4*	
Cys^{8}-Cys^{26}	925.1	1848.1	3752.2	2696.1	5522.3
			3757.7	*2698.7*	
Cys9-Cys^{42}	1027.2	3444.9	2052.2	4396.1	5420.6
		3445.2	*2052.2*		
Cys^{32}-Cys^{53}	3310.8	2261.5	957.0	5495.3	3136.6
Cys^{33}-Cys^{60}	3412.9	2964.3	148.1	6300.2	3034.4
	3415.5	*2961.2*			

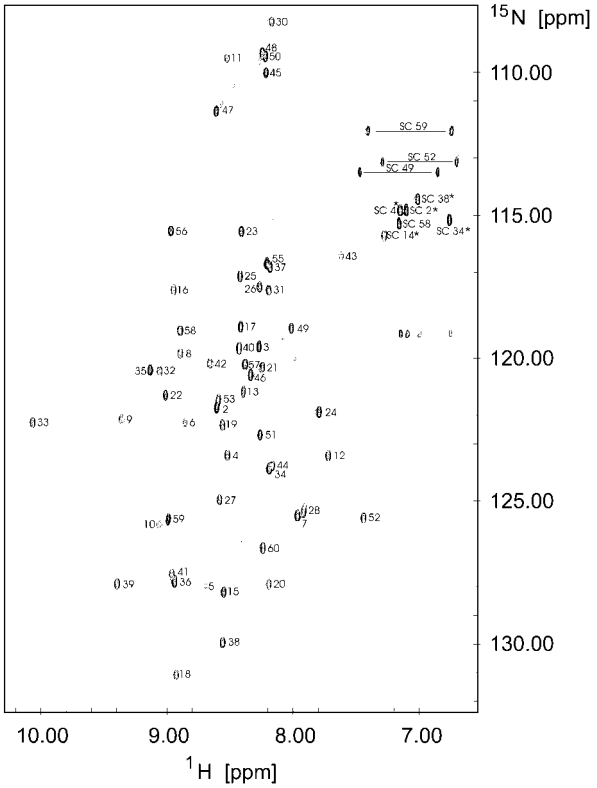

FIG. 2. **The 500 MHz ^{1}H-^{15}N HSQC spectrum of 2 mM NIP1 at 25 °C, 500 MHz.** All expected cross-peaks from 57 backbone amide protons and from 8 side chains, *i.e.* 2 Asn, 1 Gln, and 5 Arg residues, could be assigned using two-dimensional and ^{15}N-edited three-dimensional NMR spectra. They are marked by the corresponding residue number. Folded cross-peaks are marked (*).

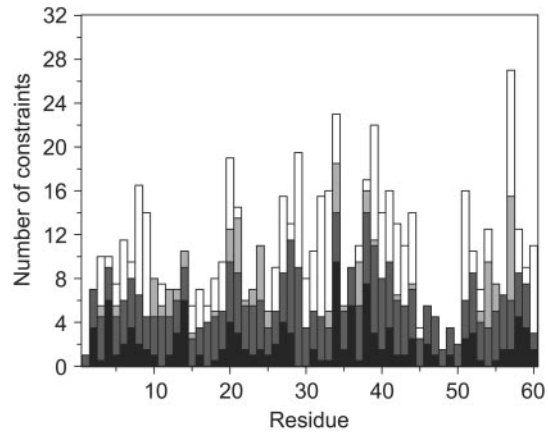

FIG. 3. **Histogram showing the number of NOE-derived distance constraints per residue.** The *bars* represent intraresidue (*black*), sequential (*dark gray*), medium range (*light gray*), and long range (*white*) NOEs restraints. From the 740 NOEs, 232 are intraresidue, 241 sequential, and 54 medium range (between 2 and 5 residues apart in the sequence). Furthermore, 213 long range NOEs (5 or more residues apart) were identified.

curs. This is supported by the observation that residues 5 and 6 in the center of β1, and residue 16 in β2, have much higher $J(0)$ values than their neighboring residues, while their $J(\omega_N)$ and $<J(\omega_H)>$ values are comparable (Fig. 5). The flexible loop between β1 and β2 (loop I, residues 9–15) is less well defined (Fig. 4, *A* and *B*). In addition, residue 13 experiences conformational exchange (Fig. 5).

Loop II, between β2 and β3, connects the two parts of the molecule. The first β-sheet ends in a type I β-turn (residues 21–24). Examination of the φ and ψ angles shows that the orientation of residues 24–28 in loop II are well defined and can be recognized as β-strand. However, no hydrogen bond partners are found for these amino acids. The exception is residue 27, the oxygen of which is hydrogen-bonded to the NH of residue 9, thereby forming an isolated β-bridge, which restricts the number of possible conformations. In addition, the cystine formed by residues 8 and 26 makes this part of the loop even more stable. Residue 9 is also the cystine partner of residue 42, providing an additional connection between the two structural motifs. The stabilized mutual orientation of the two structural motifs is further indicated by the presence of multiple NOEs between the motifs. Especially, the aromatic residue, Phe^{51}, has many interactions with residues in both parts of the molecule.

The β-sheet in the second structural motif consists of three anti-parallel β-strands; β3-(30–34), β4-(37–41), and β5-(58–59). The sheet is well defined (Fig. 4, *A* and *B*) and ends at the C terminus of the protein, where the cysteine bridge between residues 33 and 60 provides additional stability. β3 and β4 are connected by a β-turn (residues 34–37), while β4 and β5 are connected by loop III. The conformational freedom in this loop is restricted by two interactions, *i.e.* by the cystine formed by residues 32 and 53 and by the hydrogen bond between residues 44 and 51, forming another isolated β-bridge. The relaxation data indicate that the sequence comprising residues 45–51 is rather flexible. The relatively high $<J(\omega_H)>$ values indicate high frequency motions for these residues. However, the $J(0)$ values of these residues are also higher, indicating the occurrence of more complex dynamics. Loop III ends in a type II β-turn (residue 54–57).

The dynamic variation in different parts of the molecule is corroborated by the biochemical characterization of the disulfide bonds. The accessible surface, as determined by MOLMOL (35) (Table III), is large for the two sulfur atoms involved in the bridge between Cys^{3} and Cys^{19}. This bond could be reduced with significantly more ease than the other bonds. On the other hand, the sulfur atoms of Cys^{32} and Cys^{53}, which are completely buried in the interior of the protein, are inaccessible to

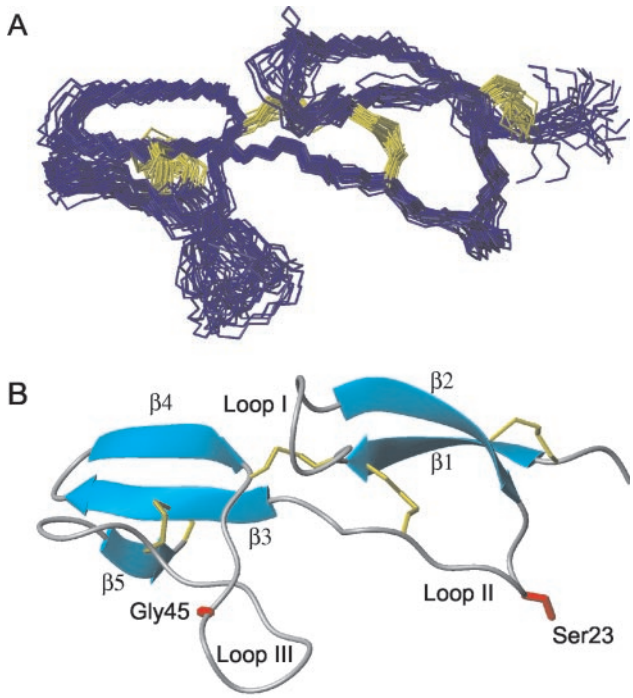

FIG. 4. **Solution structure of NIP1.** *A*, view showing best-fit superposition of the backbone atoms (N, Cα, C) of 25 structures of NIP1. The structures were overlaid for residues 3–11, 14–45, and 51–60. All cysteine bridges are depicted in *yellow*. *B*, ribbon diagram of the structure of NIP1 type I. The disulfide bridges are depicted in *yellow*. All secondary structure elements are indicated, as well as the loops and the N and C termini. The side chains specifying Ser^{23} and Gly^{45} have been colored *red*.

TABLE II
Summary of restraint violations and quality analysis for 25 NIP1 structures

DYANA target function (Å^2)	1.52 ± 0.32
Distance restraints violations	
Upper distance limit violations, average maximum (Å)	0.43 ± 0.10
Lower distance limit violations, average maximum (Å)	0.28 ± 0.08
Dihedral angle restraints violations	
Average maximum (°)	0.04 ± 0.02
Van der Waals distance restraints violations	
Average maximum (Å)	0.14 ± 0.04
Ramachandran analysis	
Most favored regions (%)	67.4
Additionally allowed regions (%)	29.5
Generally allowed regions (%)	0.9
Disallowed regions (%)	2.2
Root mean square deviations of atomic coordinates	
Backbone and heavy side-chain, all residues (Å)	1.753
Backbone, all residues (Å)	1.157
Backbone and heavy side-chain, residues 3–11, 14–45, 51–60 (Å)	1.273
Backbone, *idem* (Å)	0.660

TCEP, and no four-disulfide polypeptide species could be detected in which the disulfide bond between Cys^{32} and Cys^{53} was reduced. Even the presence of 6 M GuCl does not facilitate the TCEP reduction of this disulfide bond. Apparently, the presence of the Cys^{32}-Cys^{53} bridge, which is positioned between two strands of the anti-parallel β-sheet, strongly stabilizes the tertiary structure of this part of the protein. Also the Cys^{33}-Cys^{60} is hardly reduced by TCEP, although Cys^{60} has quite an extensive solvent accessible surface. In conclusion, the derived tertiary structure of NIP1 provides a satisfactory explanation

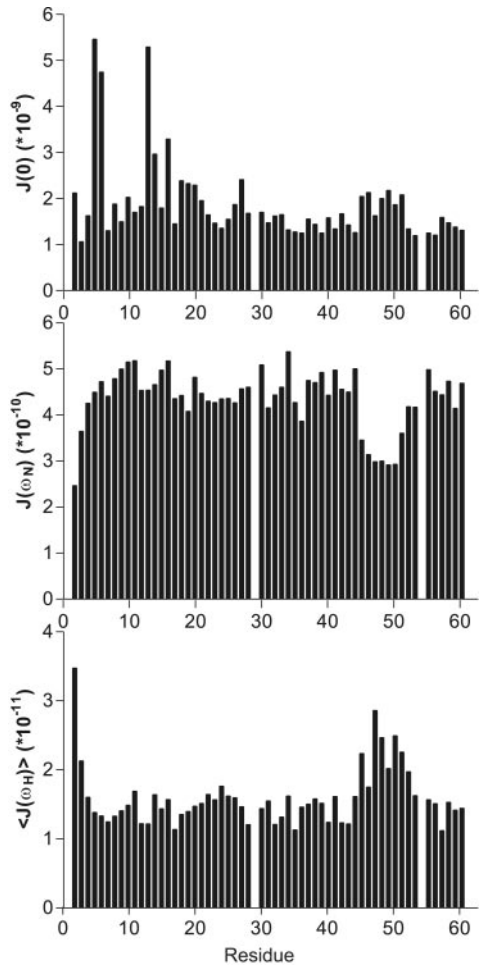

FIG. 5. **Values of the spectral density function *versus* the residue number of NIP1.** The spectral density function was determined at the frequencies 0 (*A*), ω_N (*B*), and $<J(\omega_H)>$ (*C*).

TABLE III
Solvent-accessible surface of the sulfur atoms in the final NMR structure of NIP1

Disulfide bridge	Sulfur area (Å^2) per Cys	Total area (Å^2) per Cys
Cys^3-Cys^{19}	3.0 (4.5%)–26.4(38.7%)	66.3–68.3
Cys^8-Cys^{26}	0.5 (0.7%)–2.0(2.9%)	73.3–68.3
Cys^9-Cys^{42}	0.0–8.5 (11.9%)	75.8–71.3
Cys^{32}-Cys^{53}	0.0–0.0	65.3–74.8
Cys^{33}-Cys^{60}	28.4(42.9%)–1.0(1.3%)	75.3–75.3

for the observed reduction of the individual disulfide bonds.

The NIP1 Elicitor Has a Novel Protein Fold—The disulfide pattern found in NIP1 has not been observed before in other proteins (motif.genome.ad.jp). In addition, to our knowledge the cysteine bonding pattern found in NIP1 has not been observed before in other proteins. The structure of NIP1 shows no homology to structures in the protein data bank, as was verified using the DALI server (www2.ebi.ac.uk/dali/) using a Z-score value of 2 as cut-off, nor with other elicitor proteins. For instance, the global fold of the AVR9 elicitor from the fungal tomato pathogen *C. fulvum* has been derived (36). Although the tertiary structure of the protein has not yet been completely elucidated, the presence of a cystine knot motif could be established. Furthermore, the preliminary three-dimensional structure of AVR9 shows homology to that of the carboxypeptidase inhibitor, whose structure was determined by x-ray diffraction (36, 37). The cystine knot motif was not found in NIP1. The only other structure currently available from a microbial elic-

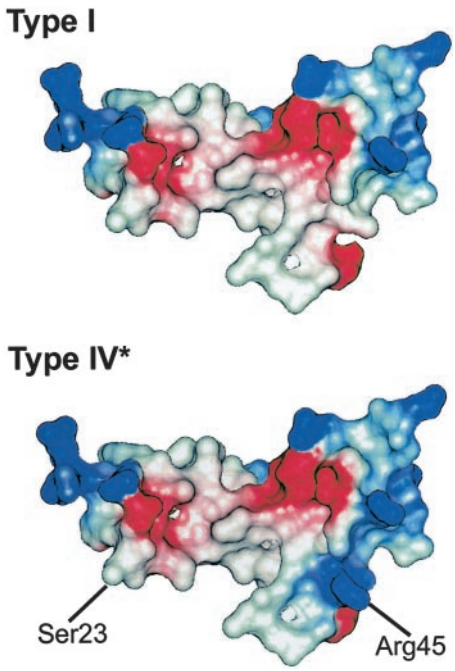

FIG. 6. **Electrostatic surface potential of NIP1 (*A*) and the G45R isoform type IV* (*B*).** Surface color reflects the sign of electrostatic potential: *red*, negative; *blue*, positive; *white*, neutral. The structure of G45R was generated by exchanging Gly^{45} by Arg in the program MOLMOL (34). Compared with Fig. 4, the structure of the protein was rotated by 180° around the *y* axis.

itor protein, that of the elicitin cryptogein (38) from *Phytophthora cryptogea*, consists mainly of α-helical elements. Other small cysteine-rich proteins, which consist of two apparent domains, such as anti-stasin (Protein Data Bank accession code 1SKZ), display dissimilar folds. Therefore, the NIP1 structure can be regarded as a novel protein fold and it may be the first representative of an evolutionary superfamily.

Structure-Function Relationship—Association of NIP1 to a binding site on *Rrs1*-barley membranes is regarded as the initiating event in a signal transduction pathway that ultimately leads to resistance. The mechanism by which this and other elicitors trigger the plant defense response remains to be fully understood. One way to address the problem is by considering the elicitor activity of NIP1 isoforms. In fungal isolates, two types of NIP1 have been identified, in which the naturally occurring amino acid alterations S23P (type III) and G45R (type IV), respectively, yield proteins that show neither elicitor nor toxic activity (12, 17). The solution NMR studies of NIP1 reported here are an important step toward an understanding of the relationships between structure and the observed biological effects.

The amino acid alteration S23P occurs at the third residue in a type I β-turn. It is well known that this type of β-turn is compatible with any amino acid residue at its four positions with one exception; a Pro residue at the third position is incompatible with type I β-turns (39). Therefore, the introduction of a Pro at this position most probably results in the disruption of the protein structure causing the loss of its activity.

The mutation G45R is positioned in the part of loop III that exhibits complex internal dynamics (see above). Changing a single surface residue, in this case glycine into arginine, may have important consequences for the local stability of the protein. This has been elegantly demonstrated for the cold shock protein from the mesophile *Bacillus subtilis*, where the introduction of one arginine at the protein surface significantly increased its stability (40). Not only the size difference, but also the introduction of a positive charge in a region, which consists of two negatively charged glutamine residues, is likely to have dramatic consequences (Fig. 6). In particular, the presence of the arginine at position 45 may reduce the flexibilty of loop III and thus affect the protein function.

Recently, a high affinity binding site for NIP1 was identified on barley plasma membranes.[1] Interestingly, when the S23P or G45R alterations were introduced into the protein both resulting mutant isoforms (type III* and type IV*), although inactive, were efficient competitors for the binding site. This indicates that the regions where the mutations had been introduced are not involved in receptor binding. However, both mutations prevent signaling to occur. It is therefore tempting to speculate that NIP1 interacts with the primary receptor through a region in the structure opposite to residues 23 and 45. Binding may induce a conformational change that allows signaling to occur through the region around amino acid residues 23 and 45. Alternatively, the latter region may attract another plant component, possibly the *Rrs1* gene product, into the signaling complex. This would be in agreement with the guard hypothesis for *R* gene function (1), which proposes that R proteins recognize the intended manipulation of a plant target by a pathogen avirulence protein. In the present case, the NIP1 receptor would be the target of the virulence function of NIP1 and hence the guardee.

Acknowledgments—The NMR measurements were performed at the Dutch National NMR Facility and at the Swedish NMR Center. J. Joordens and Ch. Damberg are acknowledged for their help. A. G. Murzin, Medical Research Council Laboratory of Molecular Biology (Cambridge, UK), is gratefully acknowledged for critically "looking at the structure."

REFERENCES

1. Dangl, J. L. & Jones, J. D. G. (2001) *Nature* **411,** 826–833
2. Cohn, J., Sessa, G. & Martin, G. B. (2001) *Curr. Opin. Immunol.* **13,** 55–62
3. van't Slot, K. A. E. & Knogge, W. (2002) *Crit. Rev. Plant Sci.* **21,** 229–271
4. van der Biezen, E. A. & Jones, J. D. G. (1998) *Trends Biochem. Sci.* **23,** 454–456
5. Mackey, D., Holt, B. F., Wiig, A. & Dangl, J. L. (2002) *Cell* **108,** 743–754
6. Galán, J. E. & Collmer, A. (1999) *Science* **284,** 1322–1328
7. Jia, Y., McAdams, S. A., Bryan, G. T., Hershey, H. P. & Valent, B. (2000) *EMBO J.* **19,** 4004–4014
8. Laugé, R. & de Wit, P. J. G. M. (1998) *Fungal Genet. Biol.* **24,** 285–297
9. Kooman-Gersmann, M., Honée, G., Bonnema, G. & de Wit, P. J. G. M. (1996) *Plant Cell* **8,** 929–938
10. Luderer, R., Rivas, S., Nürnberger, T., Mattei, B., van den Hooven, H. W., van der Hoorn, R. A. L., Romeis, T., Wehrfritz, J. M., Blume, B., Nennstiel, D., *et al.* (2001) *Mol. Plant-Microbe Interact.* **14,** 867–876
11. Rivas, S., Romeis, T. & Jones, J. D. G. (2002) *Plant Cell* **14,** 689–702
12. Rohe, M., Gierlich, A., Hermann, H., Hahn, M., Schmidt, B., Rosahl, S. & Knogge, W. (1995) *EMBO J.* **14,** 4168–4177
13. Gierlich, A., van 't Slot, K. A. E., Li, V. M., Marie, C., Hermann, H. & Knogge, W. (1999) *Protein Expression Purif.* **17,** 64–73
14. Hahn, M., Jüngling, S. & Knogge, W. (1993) *Mol. Plant-Microbe Interact.* **6,** 745–754
15. Wevelsiep, L., Kogel, K.-H. & Knogge, W. (1991) *Physiol. Mol. Plant Pathol.* **39,** 471–482
16. Wevelsiep, L., Rüpping, E. & Knogge, W. (1993) *Plant Physiol.* **101,** 297–301
17. Fiegen, M. & Knogge, W. (2002) *Physiol. Mol. Plant Pathol.* **61,** 299–302
18. Sambrook, J., Fritsch, E. F. & Maniatis, T. (1989) *Molecular Cloning: A Laboratory Manual*, Cold Spring Harbor Laboratory Press, Cold Spring Harbor, NY
19. Wu, J. & Watson, J. T. (1997) *Protein Sci.* **6,** 391–398
20. Wu, J., Gage, D. A. & Watson, J. T. (1996) *Anal. Biochem.* **235,** 161–174
21. Wu, J. & Watson, J. T. (1998) *Anal. Biochem.* **258,** 268–276
22. Delaglio, F., Grzesiek, S., Vuister, G. W., Zhu, G., Pfeifer, J. & Bax, A. (1995) *J. Biomol. NMR* **6,** 277–293
23. Bartels, C., Xia, T. H., Billeter, M., Guntert, P. & Wüthrich, K. (1995) *J. Biomol. NMR* **6,** 1–10
24. Wüthrich, K. (1986) *NMR of Proteins and Nucleic Acids*, John Wiley & Sons, New York
25. Wishart, D. S., Sykes, B. D. & Richards, F. M. (1992) *Biochemistry* **31,** 1647–1652
26. Vuister, G. W. & Bax, A. (1992) *J. Biomol. NMR* **2,** 401–405
27. Kay, L. E. & Bax, A. (1990) *J. Magn. Reson.* **86,** 110–126
28. Xia, Y. L., Kong, X. M., Ip, N. & Zhu, G. (2000) *J. Magn. Reson.* **146,** 228–231
29. Szyperski, T., Guntert, P., Otting, G. & Wüthrich, K. (1992) *J. Magn. Reson.* **99,** 552–560
30. Farrow, N. A., Muhandiram, R., Singer, A. U., Pascal, S. M., Kay, C. M., Gish, G., Shoelson, S. E., Pawson, T., Formankay, J. D. & Kay, L. E. (1994) *Biochemistry* **33,** 5984–6003

31. Palmer, A. G., Rance, M. & Wright, P. E. (1991) *J. Am. Chem. Soc.* **113,** 4371–4380
32. Guntert, P., Mumenthaler, C. & Wüthrich, K. (1997) *J. Mol. Biol.* **273,** 283–298
33. van den Hooven, H. W., van den Burg, H. A., Vossen, P., Boeren, S., de Wit, P. J. G. M. & Vervoort, J. (2001) *Biochemistry* **40,** 3458–3466
34. Degani, Y. & Patchornik, A. (1974) *Biochemistry* **13,** 1–11
35. Koradi, R., Billeter, M. & Wüthrich, K. (1996) *J. Mol. Graphics* **14,** 51–55
36. Vervoort, J., van den Hooven, H. W., Berg, A., Vossen, P., Vogelsang, R., Joosten, M. H. A. J. & de Wit, P. J. G. M. (1997) *FEBS Lett.* **404,** 153–158
37. Rees, D. C. & Lipscomb, W. N. (1982) *J. Mol. Biol.* **160,** 475–498
38. Gooley, P. R., Keniry, M. A., Dimitrov, R. A., Marsh, D. E., Keizer, D. W., Gayler, K. R. & Grant, B. R. (1998) *J. Biomol. NMR* **12,** 523–534
39. Creighton, T. E. (1983) *Proteins: Structures and Molecular Properties*, W. H. Freeman and Co., New York
40. Perl, D., Mueller, U., Heinemann, U. & Schmid, F. X. (2000) *Nat. Struct. Biol.* **7,** 380–383

Solution Structure of the Plant Disease Resistance-triggering Protein NIP1 from the Fungus *Rhynchosporium secalis* Shows a Novel β-Sheet Fold

Klaas A. E. van't Slot, Harrold A. van den Burg, Cathelijne P. A. M. Kloks, Cornelis W. Hilbers, Wolfgang Knogge and Christina H. M. Papavoine

J. Biol. Chem. 2003, 278:45730-45736.
doi: 10.1074/jbc.M308304200 originally published online August 27, 2003
